Human Brain Mapping with Conformal Geometry and Multivariate Tensor-based Morphometry

Jie Shi[1], Paul M. Thompson[2], Yalin Wang[1]

[1]School of Computing, Informatics and Decision Systems Engineering, ASU, Tempe, AZ 85281, USA
[2]Lab. of Neuro Imaging, UCLA School of Medicine, Los Angeles, CA 90095, USA
jie.shi@asu.edu

Abstract. In this paper, we introduce theories and algorithms in conformal geometry, including Riemann surface, harmonic map, holomorphic 1-form, and Ricci flow, which play important roles in computational anatomy. In order to study the deformation of brain surfaces, we introduce the multivariate tensor-based morphometry (MTBM) method for statistical computing. For application, we introduce our system for detecting Alzheimer's Disease (AD) symptoms on hippocampal surfaces with an automated surface fluid registration method, which is based on surface conformal mapping and mutual information regularized image fluid registration. Since conformal mappings are diffeomorphic and the mutual information method is able to drive a diffeomorphic flow that is adjusted to enforce appropriate surface correspondences in the surface parameter domain, combining conformal and fluid mappings will generate 3D shape correspondences that are diffeomorphic. We also incorporate in the system a novel method to compute curvatures using surface conformal parameterization. Experimental results in ADNI baseline data diagnostic group difference and APOE4 effects show that our system has better performance than other similar work in the literature.

1 Introduction

Conformal structure is an intrinsic feature of a metric surface. All oriented surfaces have conformal structures. Many recent researches have used algorithms from conformal geometry for computational analysis of brain anatomy. For brain surface flattening [7] and brain surface parameterization research, Hurdal et al. [11] reported a discrete mapping approach that uses circle packings to produce "flattened" images of cortical surfaces on the sphere, the Euclidean plane, and the hyperbolic space. The maps obtained are quasi-conformal approximations of classical conformal maps. [2] implemented a finite element approximation for parameterizing brain surfaces via conformal mappings. Gu et al. [8] proposed a method to find a unique conformal mapping between any two genus zero manifolds by minimizing the harmonic energy of the map. The holomorphic 1-form based conformal parameterization [18] can conformally parameterize high genus surface with boundaries but the resulting mappings have singularities. The Ricci

flow method [17] can handle surfaces with complicated topologies (boundaries and landmarks) without singularities.

In general, in order to study the deformation of cortical surfaces, there exist two different approaches, deformation-based morphometry (DBM) [5] and tensor-based morphometry (TBM) [6]. One advantage of TBM for surface morphometry is that it can use the intrinsic Riemannian surface metric to characterize local changes. [12, 20] proposed a new multivariate TBM framework for surface morphometry. MTBM computes statistics from the Riemannian metric tensors that retain the full information in the deformation tensor fields, thus is more powerful in detecting surface differences [20].

Using holomorphic 1-forms, a global conformal parameterization can be developed to conformally map a surface to a rectangular domain in the Euclidean plane. The mutual information (MI) method has been widely used to drive a diffeomorphic flow in image registration. By adjusting the mutual information method to enforce appropriate surface correspondences in the parameter domain, any scalar-valued signals defined on the surfaces can also be aligned using the same flow field. Conformal maps and fluid registration techniques can be combined to avoid having to define a large set of manually-defined landmarks. Since they generate diffeomorphic mappings, conformal and fluid mappings together could generate 3D shape correspondences that are diffeomorphic (i.e., smooth one-to-one correspondences). In [16], Wang et al. proposed an automated surface fluid registration method based on conformal mapping and mutual information regularized image fluid registration and applied it to register human faces and hippocampus. Here we develop a system based on this technique for studying hippocampus in Alzheimer's Disease and incorporate a novel method to compute surface curvatures as proposed in [13]. Our major contributions can be summarized as: (1). Introduction of a new stable method to compute surface curvatures. (2). An automated hippocampal surface segmentation and registration system validated in ADNI baseline data. (3). The system will be publicly available [21]. Last, although the current system finds applications in AD detection, it is a general method which may be applied to many other applications.

2 Theoretical Background

Here we briefly introduce some theories in conformal geometry. For details, we refer readers to [10] for algebraic topology and [9] for differential geometry.

2.1 Riemann Surface

Let S be a surface in $\mathbb{R}^3$ with an atlas $\{(U_\alpha, z_\alpha)\}$, where (U_α, z_α) is a coordinate chart defined on S. The atlas thus is a set of consistent charts with smooth transition functions between overlapping charts. Here $z_\alpha : U_\alpha \to \mathbb{C}$ maps an open set $U_\alpha \subset S$ to a complex plane $\mathbb{C}$. If on any chart (U_α, z_α) in the atlas, the *Riemannian metric* or the $first\ fundamental\ form$ can be formulated as $ds^2 = \lambda(z_\alpha)^2 dz_\alpha d\bar{z}_\alpha$, and the transition maps $z_\beta \circ z_\alpha^{-1} : z_\alpha(U_\alpha \bigcap U_\beta) \to z_\beta(U_\alpha \bigcap U_\beta)$ are holomorphic, the atlas could be called $conformal$. Given a conformal atlas, a chart is *compatible* with the atlas if adding this chart still generates a conformal atlas. A $conformal\ structure$ is obtained by adding all

possible compatible charts to a conformal atlas. A *Riemann surface* is a surface with a conformal structure. All metric surfaces are Riemann surfaces. Following the uniformization theorem [1], we can embed any Riemann surface onto one of the three canonical surfaces: the sphere $\mathbb{S}^2$ for genus zero surfaces with positive Euler numbers, the plane $\mathbb{E}^2$ for genus one surfaces with zero Euler numbers, and the hyperbolic space $\mathbb{H}^2$ for high genus surfaces with negative Euler numbers.

2.2 Harmonic Maps

For genus zero surfaces, the major algorithm to compute their conformal mapping is *harmonic maps*. Suppose S_1, S_2 are two metric surfaces embedded in $\mathbb{R}^3$. $\phi : S_1 \to S_2$ is a map from S_1 to S_2. The *harmonic energy*, which measures the stretching of ϕ, is defined as $E_\phi = \int_{S_1} \|\nabla\phi\|^2 dA$. A *harmonic map* is a map ϕ that minimizes the harmonic energy. It can be easily computed by the steepest descent algorithm:

$$\frac{d\phi}{dt} = -\Delta\phi \tag{1}$$

The normal component of the Laplacian $\Delta\phi$ is $\Delta\phi^\perp =< \Delta\phi, \mathbf{n}(\phi) > \mathbf{n}(\phi)$. If ϕ is a harmonic map, then we should have $\Delta\phi = \Delta\phi^\perp$. Then Eq. 1 can be solved as $\frac{d\phi}{dt} = -(\Delta\phi - \Delta\phi^\perp)$. Fig. 1 (a) shows an example of the harmonic map.

2.3 Holomorphic 1-form and Slit Mapping

Let S be a surface embedded in $\mathbb{R}^3$ with induced Euclidean metric $\mathbf{g}$. S is covered by atlas $\{(U_\alpha, z_\alpha)\}$ and (x_α, y_α) is the local parameter on a chart. Suppose ω is a differential 1-form with the representation $f(x_\alpha, y_\alpha)dx_\alpha + g(x_\alpha, y_\alpha)dy_\alpha$. ω is a *closed* 1-$form$ if on each parameter (x_α, y_α), $\frac{\partial f}{\partial y_\alpha} - \frac{\partial g}{\partial x_\alpha} = 0$. ω is an *exact* 1-$form$ if it equals to the gradient of another function defined on S. An exact 1-form is also a closed 1-form. If a closed 1-form ω satisfies $\frac{\partial f}{\partial x_\alpha} + \frac{\partial g}{\partial y_\alpha} = 0$, then ω is a *harmonic* 1-$form$. A *holomorphic* 1-$form$ is a complex differential form $\tau = \omega + \sqrt{-1}{}^*\omega$, where ω is a harmonic 1-form and ${}^*\omega = -g(x_\alpha, y_\alpha)dx_\alpha + f(x_\alpha, y_\alpha)dy_\alpha$ is the conjugate of ω, which is also a harmonic 1-form. Fig. 1 (b) shows an example of the holomorphic 1-form. Fix a point p_0 on the surface, for any point $p \in S$, let γ be an arbitrary path connecting p_0 and p, the mapping $\phi(p) = e^{\int_\gamma \tau}$ is called slit mapping. Fig. 1 (c) shows the result of slit mapping.

2.4 Ricci Flow

The Ricci flow is the process to deform a metric $\mathbf{g}(t)$ according to its induced Gaussian curvature $K(t)$, where t denotes the time parameter: $\frac{d\mathbf{g}(t)}{dt} = -K(t)\mathbf{g}(t)$. There is an analog between Ricci flow and the heat diffusion process. When Ricci flow converges, the metric $\mathbf{g}(t)$ at time t is conformal to the original metric and the Gaussian curvature is constant everywhere. Fig. 1 (d) and (e) show the results of the Euclidean and hyperbolic Ricci flow, respectively.

2.5 Multivariate Tensor Based Morphometry

Suppose $\phi : S_1 \to S_2$ is a map from surface S_1 to surface S_2. The derivative map of ϕ is the linear map between the tangent spaces, $d\phi : TM(p) \to TM(\phi(p))$, induced by the map ϕ, which also defines the Jacobian matrix of ϕ. Let J be the

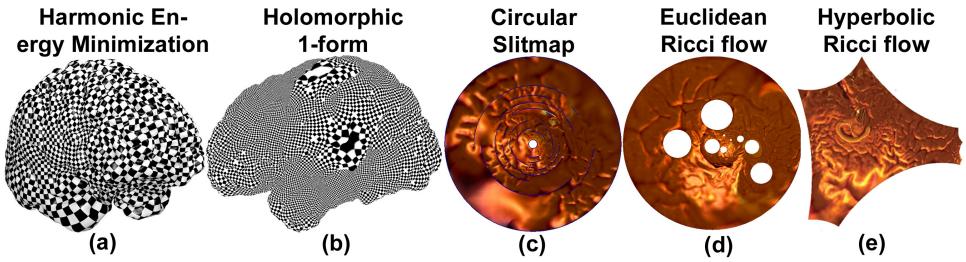

Fig. 1. Various conformal parameterization results.

Jacobian matrix and define the deformation tensors as $S = (J^T J)^{\frac{1}{2}}$. Instead of analyzing shape change based on the eigenvalues of the deformation tensors, a new family of metrics, the "Log-Euclidean metrics" [3], which are computed by inverse of matrix exponential, are considered. Hotelling's T^2 test is applied on sets of values in the Log-Euclidean space of the deformation tensors. Given two groups of n-dimensional vectors $S_i, i = 1, ..., p, T_j = 1, ..., q$, let $\bar{S}$ and $\bar{T}$ be the means of the two groups and $\sum$ is the combined covariance matrix of the two groups. The Mahalanobis distance $M = (log\bar{S} - log\bar{T}) \sum^{-1} (log\bar{S} - \bar{T})$ is used to measure the group mean difference. For details of MTBM, we refer to [12, 20].

3 Applications

Conformal geometry has broad applications in medical imaging, geometric modeling and many other fields. Recent years, we have applied it in brain surface conformal parameterization [17–19], brain surface registration [16], MRI-based biomarker detection with machine learning [22], and neonate brain study. In this section, we highlight an automated surface registration system based on the combination of surface conformal mapping and image fluid registration methods. Surface registration usually requires defining a lot of landmarks in order to align corresponding functional regions. Labeling features could be accurate but time-consuming. Here we show that surface conformal mapping could represent surface geometric features, thus avoiding the manual definition of landmarks.

For a general surface and its conformal mapping $\phi : S \to \mathbb{R}^2$, the conformal factor at a point p can be determined by the formulation: $\lambda(p) = \frac{\text{Area}(B_\epsilon(p))}{\text{Area}(\phi(B_\epsilon(p)))}$, where $B_\epsilon(p)$ is an open ball around p with a radius ϵ. The conformal factor λ encodes a lot of geometric information about the surface and can be used to compute curvatures and geodesic. In our system, we compute the surface mean curvatures only from the derivatives of the conformal parameterization as proposed in [13], instead of the three coordinate functions and the normal, which are generally more sensitive to digitization errors. Mathematically, the mean curvature is defined as:

$$H = \frac{1}{2\lambda} \text{sign}(\phi) |\Delta\phi|, \text{ where } \text{sign}(\phi) = \frac{< \Delta\phi, \overrightarrow{N} >}{|\Delta\phi|} \tag{2}$$

In this formulation of H, we need to use the surface normal $\overrightarrow{N}$ only when computing sign(ϕ), which takes the value 1 or -1. Thus, the surface normal does not

need to be accurately estimated and still we can get more accurate mean curvatures. Using the Gauss and Codazzi equations, one can prove that the conformal factor and mean curvature uniquely determine a closed surface in $\mathbb{R}^3$, up to a rigid motion. We call them the *conformal representation* of the surface. Since conformal factor and mean curvature could represent important surface features and are intrinsic to the surface, they may be used for surface registration.

After computing intrinsic geometric features, we align surfaces in the parameter domain with a fluid registration technique.Using conformal mapping, we essentially convert the surface registration problem to an image registration problem. In [16], Wang et al. proposed an automated surface fluid registration method combining conformal mapping and image fluid registration. Since conformal mapping and MI regularized fluid registration generate diffeomorphic mappings, a diffeomorphic surface-to-surface mapping is then recovered that matches surfaces in 3D. In our system, we adopt their methods of conformal mapping and fluid registration. However, our system differs from theirs in the computation of surface features as introduced above. The new way to compute mean curvature is more stable and less sensitive to normal computation, thus gives better representation of the surface features for registration.

4 Experimental Results

We applied our surface registration system to study hippocampal surface morphometry in AD. In our study, we tested the system on the Alzheimer's Disease Neuroimaging Initiative (ADNI) baseline data (http://www.loni.ucla.edu/ADNI). The data contains 233 healthy controls, 410 subjects with mild cognitive impairment (MCI), and 200 patients with AD. The hippocampal surfaces were automatically segmented using FIRST (http://www.fmrib.ox.ac.uk/fsl/fsl/list.html). FIRST is an integrated registration and segmentation tool developed as part of the FSL library, which is written mainly by members of the Analysis Group, FMRIB, Oxford, UK. We also took FIRST's technique of registration for a comparison in our diagnostic group difference study. In the segmentation step, 1 subject in each group (AD, MCI, and control) failed probably due to the original images' resolution or contrast. We also manually occluded 1 subject from the control group and 2 subjects from the MCI group because of name duplication. For subjects with duplicated names, we retained the one which was the repeated scan. Thus 837 subjects were involved in all the experiments in this paper.

In our system, we left two holes at the front and back of the hippocampal surface, representing its anterior junction with the amygdala, and its posterior limit as it turns into the white matter of the fornix. The resulting structure can then be logically represented as an open boundary genus one surface, i.e., a cylinder. Then the surfaces were conformally mapped to a rectangle plane using holomorphic 1-forms.To better visualize the matching of surface features, we chose to encode surface features using a compound scalar function based on the local conformal factor and the mean curvature. After the cross-subject registration was computed with one target surface selected, we examined shape differences using the MTBM as introduced in Sec. 2.5.

4.1 Effects of APOE4 Genotype

In [14], Morra et.al. discussed that in healthy elderly subjects, presence of the Apolipoprotein E $\epsilon 4$ allele (APOE4) may be correlated with future development of AD. In order to investigate this correlation, the authors designed two experiments: (1) group difference between APOE4 carriers and non-carriers in all samples; (2) group difference between APOE4 carriers and non-carriers in subjects that have not developed AD, i.e., MCI and control groups. The experiments are aimed to determine if the APOE4 allele is linked with hippocampal atrophy in all subjects and in just the non-AD subjects, respectively. In [14], 400 subjects with 100 AD, 200 MCI, and 100 control subjects from ADNI baseline data were studied. However, no significance was reported in [14]. In our study, among the 837 subjects, 738 subjects have been diagnosed as APOE4 carriers or non-carriers, 566 of which are MCI or controls. Fig. 2 shows the significance maps for APOE4 effects. With MTBM, our system has been able to detect more significant areas compared with [14]. The significant p-values are 0.00044 for the all-sample experiment and 0.02073 for the non-AD experiment, respectively.

In [15], Pievani et al. designed more systematic experiments to study APOE4 effects. We will study their findings in our ongoing work.

4.2 Diagnostic Group Differences

Fig. 3 illustrates the experimental results showing difference maps among the three diagnostic groups (AD, MCI and control). MCI is an intermediate stage between the expected cognitive decline of normal aging and the more pronounced decline of dementia. If MCI could be found and treated, the risk of AD will be significantly reduced. However, at MCI stage, changes in brain surface are not significant thus impose more difficulty on the detection. With MTBM, we can see that, in the three experiments, our system demonstrated better results than FIRST. Particularly, our system gave better MCI detection results when comparing with both AD and control subjects. In the experiment, all group difference p-maps were corrected using false discovery rate (FDR) [4]. The FDR method decides whether a threshold can be assigned to the statistical map that keeps the expected FDR below 5% (i.e., no more than 5% of the voxels are false positive findings). The CDF plots show the uncorrected p-values (as in a conventional FDR analysis). The x value at which the CDF plot intersects the $y = 20x$ line represents the highest statistical threshold that can be applied to the data, for which at most 5% false positives are expected in the map. The use of the $y = 20x$ line is related to the fact that significance is declared when the volume of suprathreshold statistics is more than 20 times that expected under the null hypothesis. Table 1 gives the FDR corrected p-values comparison.

5 Conclusion and Future Work

This paper reviews some algorithms in conformal geometry and highlights an automated surface fluid registration system. Experiments on ADNI hippocampal dataset demonstrate our system's stronger statistical power than other work in the literature. Ongoing work is to apply this system to automatically map lateral ventricle enlargements in Alzheimers disease and those at risk.

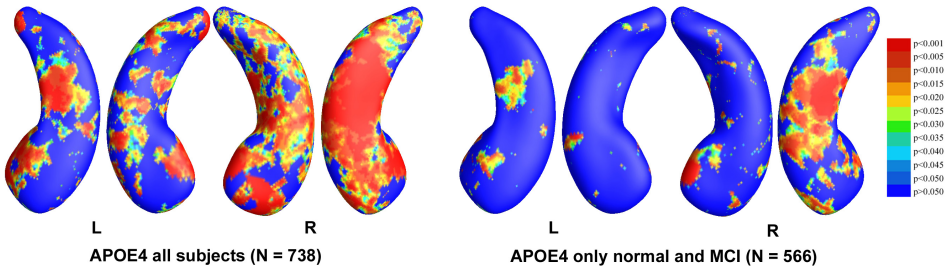

Fig. 2. Significance maps for APOE4 effects.

References

1. Abikoff, W.: The uniformization theorem. The American Mathematical Monthly 88(8), 574–592 (1981)
2. Angenent, S., et al: Conformal geometry and brain flattening. In: Med. Image Comput. Comput.-Assist. Intervention. pp. 271–278 (1999)
3. Arsigny, V., et al: Log-Euclidean metrics for fast and simple calculus on diffusion tensors. Magn. Reson. Med. 56(2), 411–421 (2006)
4. Benjamini, Y., et al: Controlling the false discovery rate: a practical and powerful approach to multiple testing. J. of the Royal Statistical Society 57, 289–300 (1995)
5. Chung, M.K., et al: Deformation-based surface morphometry applied to gray matter deformation. NeuroImage 18(2), 198–213 (2003)
6. Chung, M.K., et al: Tensor-based cortical surface morphometry via weighted spherical harmonic representation. IEEE Trans. Med. Imag. 27(8), 1143–1151 (2008)
7. Fischl, B., et al: Cortical surface-based analysis II: Inflation, flattening, and a surface-based coordinate system. NeuroImage 9(2), 195–207 (1999)
8. Gu, X., et al: Genus zero surface conformal mapping and its application to brain surface mapping. IEEE Trans. Med. Imag. 23(8), 949–958 (2004)
9. Guggenheimer, H.W.: Differential Geometry. Dover Publications (1977)
10. Hatcher, A.: Algebraic Topology. Camerbridge University Press (2006)
11. Hurdal, M.K., et al: Cortical cartography using the discrete conformal approach of circle packings. NeuroImage 23, S119–S128 (2004)
12. Leporé, N., et al: Multivariate statistics of the Jacobian matrices in tensor-based morphometry and their applications to HIV/AIDS. In: Med. Image Comput. Comput.-Assist. Intervention. pp. 191–198 (2006)
13. Lui, L.M., et al: Computation of curvatures using conformal parameterization. Communications in Information and Systems 8(1), 1–16 (2008)
14. Morra, J.H., et al: Automated 3D mapping of hippocampal atrophy and its clinical correlates in 400 subjects with Alzheimer's disease, mild cognitive impairment, and elderly controls. Human Brain Mapping 30(9), 2766–2788 (2009)

	Surface MI	FIRST
AD-CTL	0.0485	0.0419
AD-MCI	0.0215	0.0131
CTL-MCI	0.0483	0.0261

Table 1. FDR corrected p-values on hippocampal surfaces

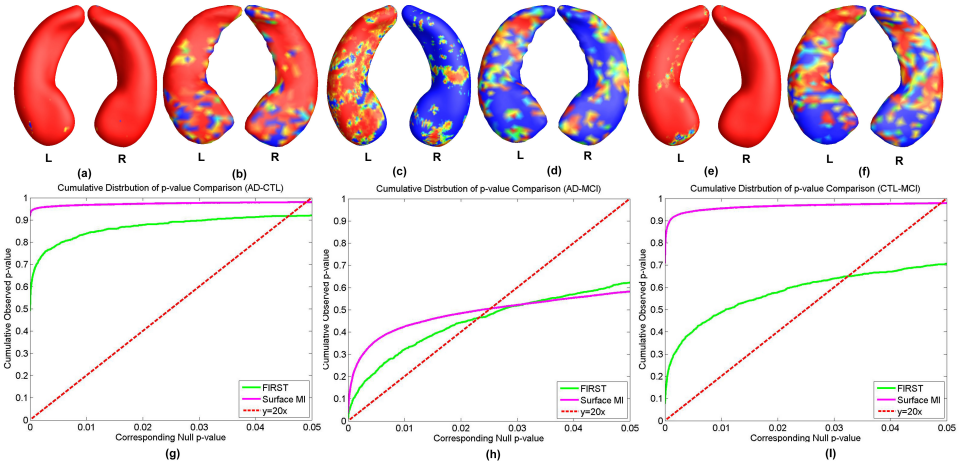

Fig. 3. Comparison of surface fluid registration and FIRST on map of local shape differences (p-values) between different diagnostic groups, based on the mutivariate TBM method with hippocampal surfaces in 199 AD, 407 MCI, and 231 control subjects which were automatically segmented by FIRST. (a), (c), (e) are our results on group difference between AD and control, AD and MCI, MCI and control, respectively. Similarly, (b), (d), (f) are results of FIRST on AD and control, AD and MCI, MCI and control, respectively. The p-map color scale is the same as Fig. 2. (g), (h), (i) are the CDF plots showing the comparisons.

15. Pievani, M., et al: APOE4 is associated with greater atrophy of the hippocampal formation in Alzheimer's disease. NeuroImage 55, 909–919 (2011)
16. Wang, Y., et al: Mutual information-based 3D surface matching with applications to face recognition and brain mapping. In: Proc. Intl Conf. Computer Vision. pp. 527–534 (2005)
17. Wang, Y., et al: Brain surface parameterization with algebraic functions. In: Med. Image Comput. Comput.-Assist. Intervention. pp. 946–954 (2006)
18. Wang, Y., et al: Brain surface conformal parameterization using Riemann surface structure. IEEE Trans. Med. Imag. 26(6), 853–865 (June 2007)
19. Wang, Y., et al: Conformal slit mapping and its application to brain surface parameterization. In: Med. Image Comput. Comput.-Assist. Intervention. pp. 585–593 (2008)
20. Wang, Y., et al: Multivariate tensor-based brain anatomical surface morphometry via holomorphic one-forms. In: Med. Image Comput. Comput.-Assist. Intervention (2009)
21. Wang, Y.: Multivariate tensor-based subcortical morphometry system (2011), http://gsl.lab.asu.edu/conformal.htm
22. Wang, Y., et al: MRI-based biomarker detection using conformal slit maps and machine learning. In: 16th Annual Meeting of the Organization for Human Brain Mapping (2010)